

## Nitrogen Doping of Porous Carbon Electrodes Derived from Pine Nut Shell for High-Performance Supercapacitors

Jinghua Li<sup>#</sup>, Xianyong Hong<sup>#</sup>, Yumei Luo, Yu Zhu, Leilei Lu, Bin Li, Fen Xu\*, Lixian Sun\*

Guangxi Key Laboratory of Information Materials & Guangxi Collaborative Innovation Centre of Structure and Property for New Energy and Materials, School of Material Science and Engineering, Guilin University of Electronic Technology, Guilin 541004, P. R. China

\*They contributed equally to this work.

\*E-mail: [sunlx@guet.edu.cn](mailto:sunlx@guet.edu.cn), [xufen@guet.edu.cn](mailto:xufen@guet.edu.cn)

Received: 6 October 2019 / Accepted: 1 December 2019 / Published: 10 June 2020

Porous carbon materials are one of the most widely studied electrode materials in supercapacitor electrode materials. Many studies have shown that increasing the specific surface area of porous carbon materials, increasing the pore structure, and hetero-atom doping can improve the electrochemical performance of porous carbon materials. Here, three-dimensional-graded porous carbon materials were successfully prepared by carbonization and activation using pine nut shells as carbon sources. After activation by potassium hydroxide, the specific surface area is as high as 2192 m<sup>2</sup>/g and the pore volume is 1.4 nm. As a supercapacitor electrode material, the specific capacitance at a current density of 0.5 A/g is as high as 408 F/g. The material also has good cycle stability (the specific capacity retention rate after 5,000 cycles of testing at a current density of 10 A/g was 95%). The large specific surface area, outstanding specific capacitance, and good cycle stability make the pine nut-shell porous carbon material a potential supercapacitor electrode material

**Keywords:** Biomass; Nitrogen doping; Porous carbon; Supercapacitors

### 1. INTRODUCTION

The energy crisis is increasingly serious [1–4]. The search for new renewable energy and environmentally friendly energy storage equipment is an important goal [5, 6]. Among various energy storage components, supercapacitors have attracted much attention in recent years because of their good power density, fast charging process, long cycle life, as well as good safety and reliability [7–10]. The electric double-layer capacitor is an important energy storage device [2, 11]. It consists of two activated carbon electrodes, and the charge energy is absorbed by the electrode material to achieve the

energy storage effect. Therefore, obtaining electrode materials with high specific surface area and high specific capacity is crucial for realizing efficient new energy storage equipment.

Activated carbon[12], carbon nanotubes[13], carbon microspheres[14], carbon onion[15]and metal oxides/nitrides are often used as electrode materials for supercapacitors. Versus other materials, activated carbon materials have attracted much attention due to their low cost, large specific surface area, good electrical conductivity, and corrosion resistance [16–18]. Traditionally, activated carbon materials have been produced primarily from expensive and non-renewable resources such as coal, petroleum, and their derivatives. Considering the potential scalability and sustainability of supercapacitors, it is important to develop low-cost carbon materials from renewable raw materials. Moreover, incineration in waste biomass resources usually produces large amounts of CO, CO<sub>2</sub>, NO<sub>x</sub>, or SO<sub>x</sub>, and the large emissions of these gases often lead to significant air pollution[19]. Therefore, the rational use of biological waste has great practical value.

For example, Wang et al. [17] used catkins as the carbon source to prepare a three-dimensional micron-sized macroporous layer structure by KOH activation. However, the specific surface area of the material is small, and the target of increasing the specific capacity of the material cannot be achieved. Wang et al. [20] prepared a three-dimensional porous carbon material via hydrothermal and carbonization using orange peel as a carbon source, but the specific surface area of the same material was only 860 m<sup>2</sup>/g. The smaller specific surface area does not provide enough space for charge adsorption during charge and discharge; thus, an increase in specific capacitance cannot be achieved. Therefore, the specific surface area remains the biggest challenge when biomass materials are used as carbon sources. Furthermore, the chemical components of biomass precursors other than carbon need to be highly valued, because heteroatoms can improve the electrochemical properties of materials by improving the surface Faraday reaction[21–23].

Here, pine nut shells were used as a carbon source, and the pre-carbonization treatment of the biomass material was realized via low-temperature carbonization in nitrogen. Urea was then used as a nitrogen source, and KOH was used to activate the materials at 600°C, 700°C, and 800°C, respectively. Finally, three-dimensional graded porous carbon materials were obtained by washing and drying. The material has a good morphology structure, a large specific surface area (2192 m<sup>2</sup>/g), and a rich pore structure. The electrochemical properties of the material were tested and found to have a specific capacitance of 408 F/g at a current density of 0.5 A/g. The material also has good cycling performance: the specific capacitance retention is 95% after 5000 cycles at a current density of 10 A/g. This good structural morphology and excellent electrochemical properties prove that the pine nut shell-based biomass materials have great potential in applications of supercapacitor electrode materials.

## 2. EXPERIMENTAL

### 2.1 Synthesis of Materials

First, the collected pine nut shells were washed with alcohol and placed in a drying oven at 80°C for 12 h. The dried pine nut shells were then ground into a powder, and the powder was heated to

350°C at a rate of 5°C/min in a nitrogen atmosphere for a pre-carbonization treatment. Second, the pre-carbonized sample was mixed with potassium hydroxide and urea at a mass ratio of 1:1:1, and 60 ml deionized water was added to the sample. The mixture was stirred continuously at room temperature and placed in a drying chamber for 24 hours. Finally, the dried mixture was activated at a heating rate of 3°C/min in nitrogen at 600 to 800°C. The samples were washed and dried and named NPC-x (x = 600, 700, 800).

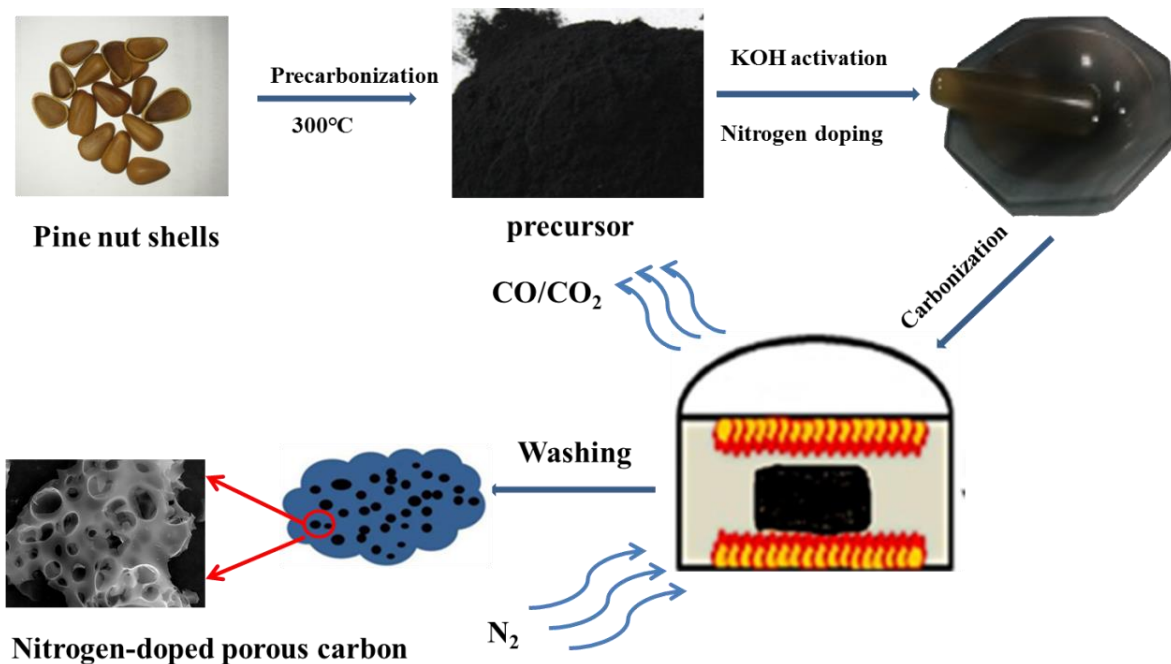


**Figure 1.** Schematic for the preparation of NPC-x.

## 2.2 Characterization of the Materials

The microstructure of the NPC was analyzed by scanning electron microscopy (FE-SEM, FEI Tecnai-450, USA) and high-resolution transmission electron microscopy (TEM, Hitachi JSM-1200EX, JEOL Ltd, Japan) equipped with an energy-dispersive X-ray spectrometer (EDS). X-ray diffraction (XRD) patterns were obtained via an X-ray diffractometer (XRD, D8 Advance, Germany). The pore structure was determined by nitrogen adsorption/desorption isotherms at 77 K (Autosorb iQ<sub>2</sub>, Quantachrome sorptometer, USA). The pore size distribution (PSD) was analyzed using the BJH model. The specific surface area (SSA) was calculated by the Brunauer–Emmett–Teller (BET) equation. The structure of the carbon materials was characterized by Raman spectrometer (UK). An X-ray photoelectron spectrometer (XPS, Thermo Scientific Escalab 250Xi, USA) was used to characterize the chemical composition.

## 2.3 Electrochemical measurement

Electrochemical analyses were performed using a three-electrode system equipped with a Hg/HgO reference electrode and a platinum counter electrode. The chemical properties of the material

were characterized by cyclic voltammetry (CV) at different scanning rates. Galvanostatic characterization (GCD) was done at different current densities along with electrochemical impedance (EIS) measurements. The specific capacitance ( $C$ , F/g), energy density ( $E$ , Wh/kg), and power density ( $P$ , W/kg) were calculated according to the following formulae:

$$C = \frac{I\Delta t}{m\Delta C}$$

$$E = \frac{C\Delta V^2}{2}$$

$$P = \frac{E}{\Delta P}$$

Here,  $C$  represents the specific capacitance of NPCs as the electrode material,  $I$  is the discharge current (A/g),  $\Delta t$  is the discharge time (s),  $m$  is the mass of the active material (g), and  $\Delta V$  is the window voltage (V).

### 3. RESULTS AND DISCUSSION

The structure of the sample was characterized by XRD, and the results are shown in Figure 2. The diffraction peaks are at  $2\theta=22.3^\circ$  and  $43.5^\circ$  corresponding to (002) and (100) crystal planes, respectively, indicating that the carbon material is amorphous graphite carbon structure with low crystallinity. Figure 2b shows the Raman spectroscopic data. The D peak represents the defect of the carbon atom lattice, and the G peak represents the in-plane stretching vibration of the carbon atom sp<sup>2</sup> hybridization. The relationship between the two peaks is usually expressed by the intensity of the peak. In general, the intensity ratio of the D peak to the G peak ( $I_D/I_G$ ) is used to indicate the degree of defects in the carbon material, that is, a larger ratio implies more lattice defects. The  $I_D/I_G$  of PNC-600, PNC-700, and PNC-800 are 0.98, 0.87, and 0.97, respectively. This means that more defects will be produced at higher activation temperatures. A larger ratio value leads to a smaller graphitization degree of carbon materials. A higher degree of graphitization increases the stability of the carbon materials[24].

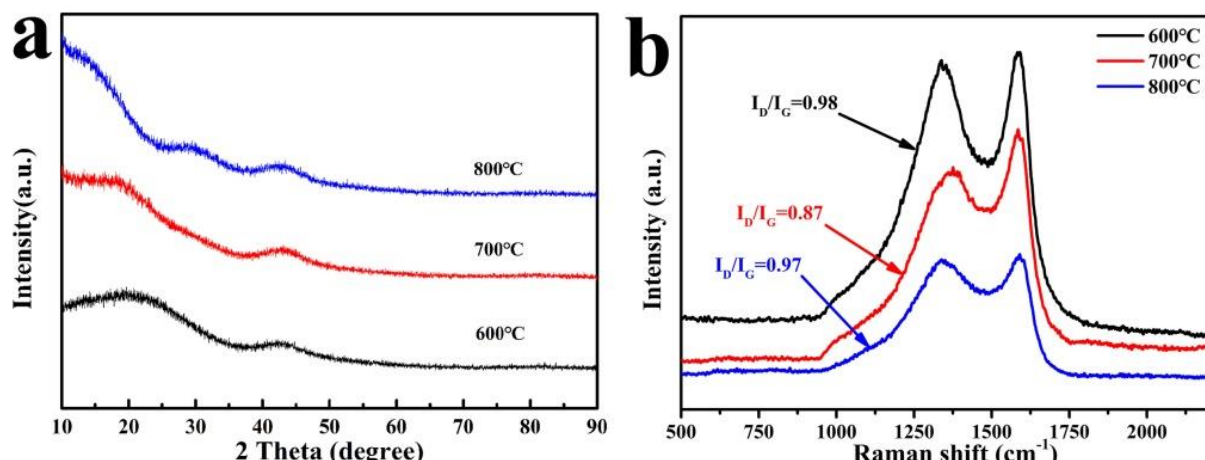


**Figure 2.** (a) XRD pattern of the NPC-x. (b) Raman spectra of the NPC-600, NPC-700, and NPC-800.

The detailed elemental composition and valence states of the PNC were further studied by XPS analysis (Fig. 3a). The full spectrum of XPS shows that all samples contain three distinct peaks corresponding to C (284.8 eV), N (400.0 eV), and O (532.8 eV), indicating that nitrogen has been successfully doped into the samples. Figure 3b-d shows the narrow spectrum of C 1s, N 1s, and O 1s in NPC-700, respectively. Figure 3b shows that three different types of carbon can be found. Their peaks correspond to 284.9 eV, 285.4 eV, and 288.1 eV, respectively. They correspond to C–C, C–N, and C=O groups. The N 1s spectrum can be divided into four peaks in different environments: pyridine nitrogen near 398.7 eV, pyrrole nitrogen near 399.6 eV, graphite nitrogen near 401.8 eV, and pyridine nitrogen oxide near 403.0 eV. N 1s XPS spectra of NPC-700 could be deconvoluted into four peaks at 398.5, 399.2, 400.8, and 403.5 eV, which are attributed to pyridinic nitrogen, pyrrolic nitrogen, quaternary nitrogen, and oxidized nitrogen, respectively[25]. The N bonded with  $sp^2$  carbon atoms in quaternary nitrogen atoms will increase the electrical conductivity of carbon materials due to the presence of extra free electrons because most quaternary nitrogen atoms are located inside the graphite-type carbon planes that break the degree of graphitization[26]. However, the pyridinic nitrogen and pyrrolic nitrogen atoms located at the edge of the carbon layers introduce a large amount of surface defects to develop a disordered honeycomb carbon structure, which is more efficacious in adsorbing heteroatoms and enhancing electron storage capacity[27–29].

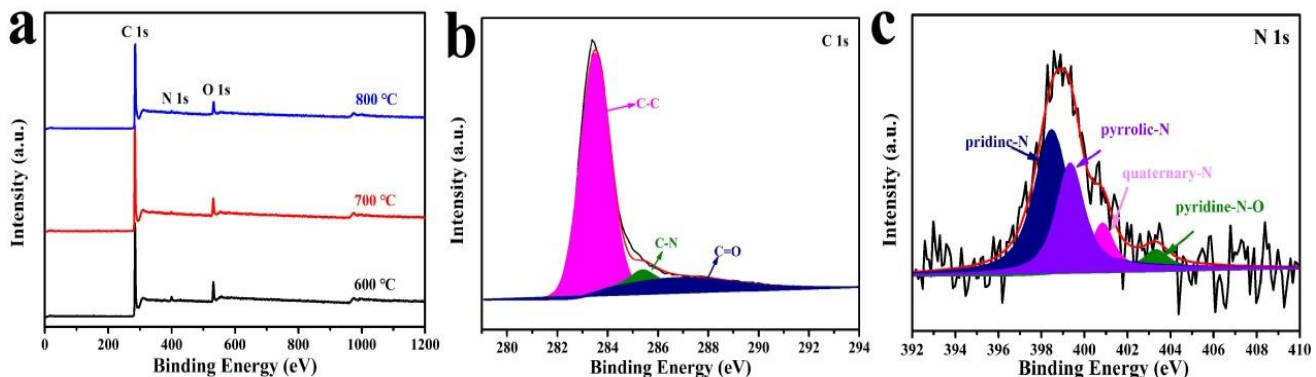


**Figure 3.** XPS spectra of (a) survey spectra, (b) C 1s, and (c) N1s.

The microstructure of the material was studied by SEM. Figure 4 shows a microscopic topography of a nitrogen-doped porous carbon material prepared at different activation temperatures. When the activation temperature was 600°C, no pore structure was formed on the surface of the sample, indicating that the temperature could not achieve the purpose of pore formation. When the temperature was raised to 700°C, the sample showed many pore structures: The pore structure was rich and the surface was smooth (Fig. 4b). There were many micropores and mesopores on the surface of the sample as well as many interconnected pore structures that increase the efficiency of the electrochemical reaction.

Mesopores and interconnections of the carbon materials are known to provide a favorable path for transportation and penetration of electrolyte ions, which is important for fast ion transfer [30]. Figure 4c shows the sample at 800°C—its structure significantly collapsed. This structure is unstable and is not conducive to the occurrence of late electrochemical reactions. The good pore structure of

NPC-700 constitutes a three-dimensional porous structure, and the HAADF image offers further proof of this (Fig. 4d). The elemental mapping of C, N, and O in NPC-700 are disclosed in Fig. 4e–g. The existence and uniform distribution of C, N, and O was observed in the surface of NPC-700, indicating that the N was successfully incorporated onto the surface of pine nut shell by thermal activation.

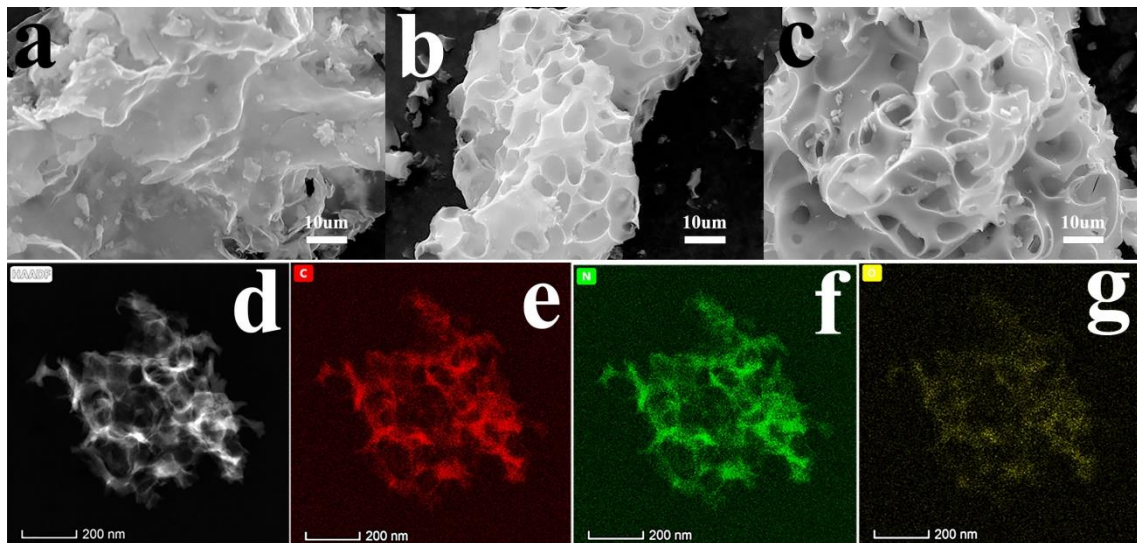


**Figure 4.** SEM images of the as-prepared NPC-x: (a) NPC-600, (b) NPC-700, and (c) NPC-800. (d) HAADF images for the NPC-700. EDX mapping result from the NPC-700: (e) C, (f) N, and (e) O.

In addition to heteroatom doping, the specific surface area and porosity is an important index that affects the energy storage performance of carbon materials. In order to study the surface area and void fraction of the sample, the sample was studied by nitrogen adsorption and desorption analysis (Figure 5). Figure 5a shows a nitrogen adsorption–desorption curve of NPC-600, NPC-700, and NPC-800, indicating that all three samples exhibit a typical type IV adsorption/desorption isotherm curve, and the curve rises sharply in the low  $P/P_0$  range. A significant hysteresis loop appears in the curve when  $P/P_0 > 0.2$ , indicating the presence of abundant micropores and mesopores in the material[32]. In addition, the continuous rise in the high  $P/P_0$  range indicates the existence of red fruit voids. Moreover, NPC-700 exhibits a larger specific surface area ( $2192 \text{ m}^2/\text{g}$ ) and total pore volume.

Versus other biomass-derived porous carbon materials, pine nut shell-based porous carbon materials have higher specific surface area because of the block structure of the original pine nut shell-based carbon materials themselves. These materials are activated at high temperatures in alkaline environment resulting in more holes. This increases the specific surface area of the materials. However, when the activation temperature is  $600^\circ\text{C}$ , the specific surface area of the material is only  $746 \text{ m}^2/\text{g}$ , indicating that the lower temperature does not provide more energy for activation at a lower activation temperature. Thus, the pores cannot be opened, and the specific surface area is lower. When the activation temperature is  $800^\circ\text{C}$ , the specific surface area of the material is  $1772 \text{ m}^2/\text{g}$ . This indicates that the material activation temperature is too high, and the structure of the material is destroyed resulting in a decrease in the ratio. The test results are consistent with SEM.

The pore size distribution of the material was also analyzed by BJH method (Fig. 5b), and the pore size distribution was about 1-3 nm. It is clear from the figure that the sample contains many micropores and mesopores. The abundant micropore structure can shorten the distance between the electrode surface and the ion center, and increase the charge transfer rate. A large number of mesoporous structures can provide channels for the transfer of electrolyte to increase the effective contact between electrolyte and the electrode thus improving the energy storage performance of the materials.

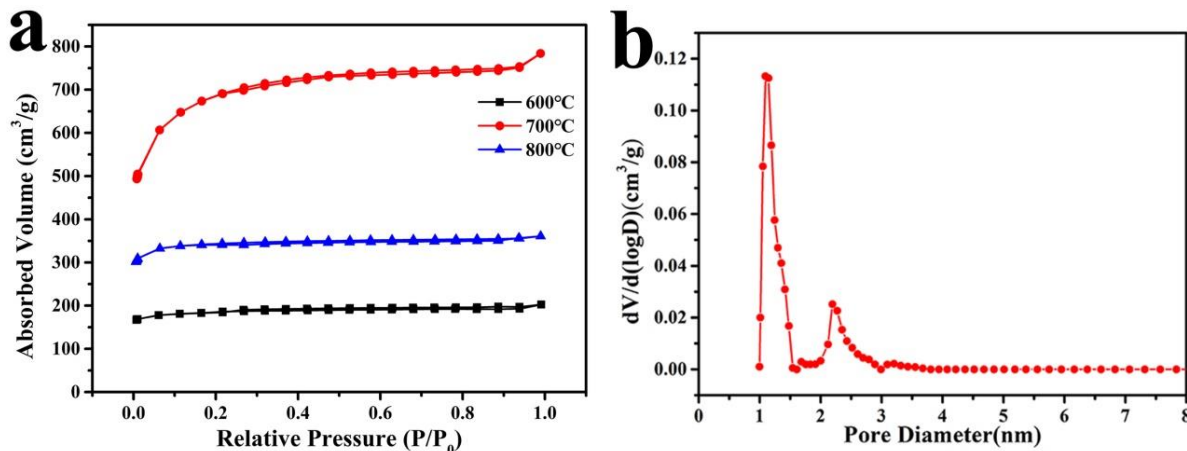


**Figure 5.** (a) Nitrogen adsorption-desorption isotherms of NPC-600, NPC-700, and NPC-800. (b) Pore size distribution plots of NPC-700.

According to the literature, nitrogen doping can improve the wettability of materials. Good wettability is conducive to the rapid diffusion of electrolytes, thereby improving the capacitance performance of materials. To verify the electrochemical properties of the materials, the electrochemical properties of the materials were characterized with 6 M KOH as an electrolyte in a three-electrode testing system. Figure 6a shows a CV curve of the NPC-x at a scan rate of 100 mV/s with a window voltage of 1 V. The area enclosed by NPC-700 is larger under the same test conditions, indicating that NPC-700 has a larger specific capacity.

Figure 6b shows the test results of all the samples. These results indicate that the GCD curves of the samples have good symmetry; thus, the material has good charge and discharge performance. The longer charge and discharge times of the NPC-700 indicate that the material has a better specific capacity, which is consistent with the larger specific surface area of the NPC-700. The Nyquist plots of NPC-600, NPC-700, and NPC-800 are depicted in Fig. 6c. The Nyquist plot is composed of two parts: an arc in the high frequency region and a vertical line in the low frequency region. Normally, the diameter of the high frequency semicircle is considered to be charge transfer resistance that proceeds at the interface of electrode/electrolyte [33]. The straight line in the low frequency region represents the capacitive behavior of the electrode, i.e., a larger slope of the straight line implies better capacitive behavior. The straight line of the NPC-700 electrode in the figure has a larger slope, indicating that the ion diffusion behavior is better. Obviously, the NPC-700 composite shows the lowest Rct.

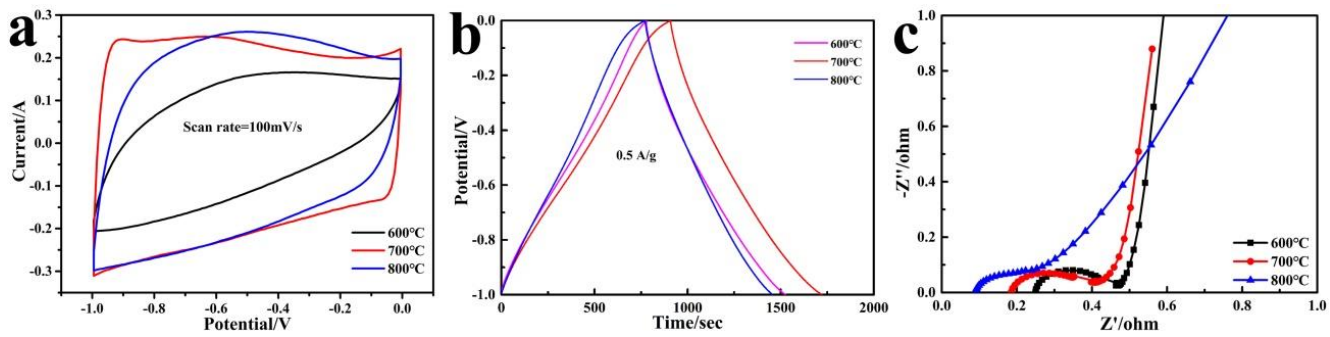


**Figure 6.** (a) CV curves of the samples at a scan rate of 100 mV/s. (b) GCD curves of the samples at a current density of 0.5 A/g. (c) Nyquist plots of the samples.

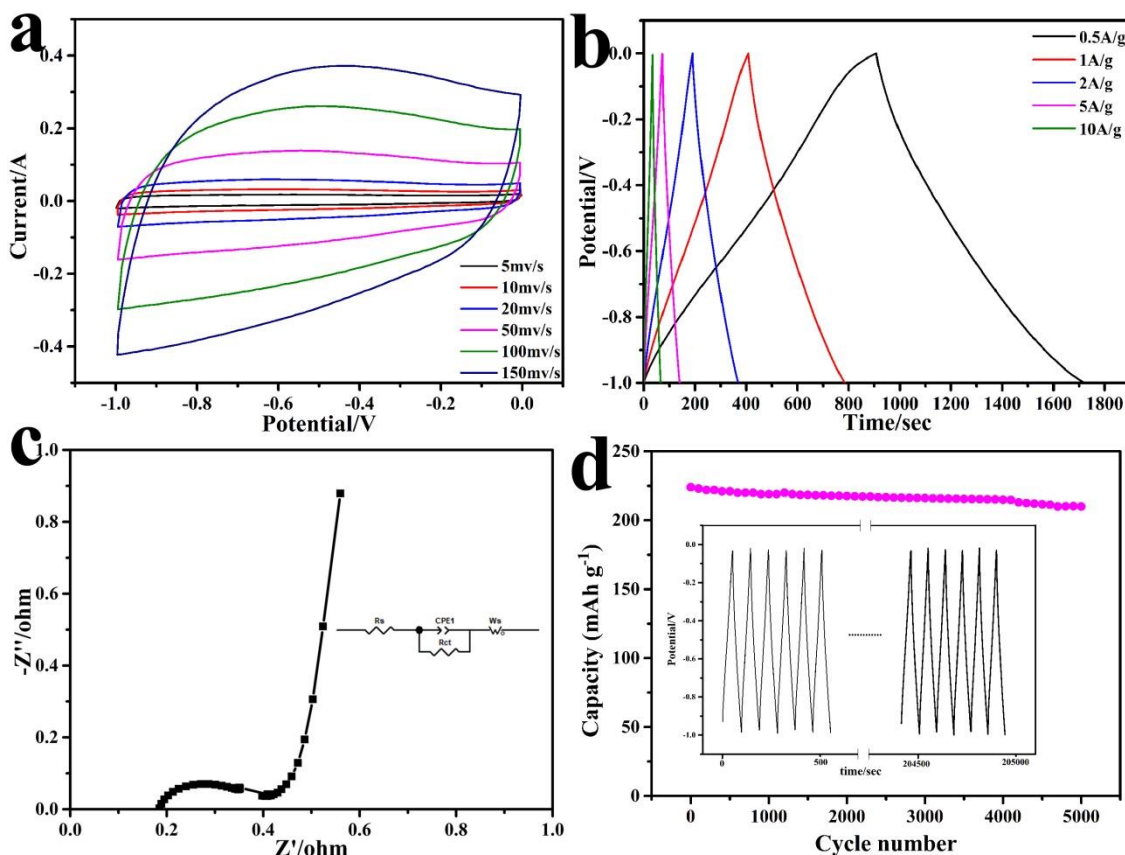


**Figure 7.** CV curves of the NPC-700 at different scan rates. (b) GCD curves of the NPC-700 at different current densities. (c) EIS Nyquist plots of the NPC-700. The insets are the corresponding equivalent circuit. (d) Cycling performance of the NPC-700 electrode at a current density of 10A/g; The inset is the first five cycles and the last five cycles.

Next, a constant current charge and discharge experiment was carried out to further study the electrochemical behavior of NPC-700. Figure 7a is a CV curve of the NPC-700 at a scan rate of 5–150

mv/s. The CV curve has a good quasi-rectangular shape, and there is a small peak around 0.2 V during charging. A similar peak appears at 0.8 V during discharge, indicating that the material undergoes tantalum capacitance during charge and discharge due to the internal nitrogen doping of the material. The CV curve maintains a good shape as the scan rate increases, suggesting that the material has good rate performance.

The NPC-700 electrode material was tested at current densities of 0.5, 1, 2, 5, and 10 A/g with specific capacitances of 408 F/g, 377 F/g, 357 F/g, 340 F/g, and 320 F/g, respectively (Figure 7b). As the current density increases, the specific capacity of the material decreases slightly suggesting that the material has a better specific capacitance retention ratio and exhibits good rate performance. The electrode materials were further studied by electrochemical impedance spectroscopy.

Figure 7c shows the Nyquist diagram of NPC-700. The equivalent series resistance of NPC-700 is 0.19 Ω. The lower equivalent series resistance indicates a higher charge transfer rate between the active electrode material and the electrolyte. Moreover, NPC-700 electrode has excellent cycling performance (specific capacity retention rate is 95% after 5000 cycles at 10A/g current density) (Fig. 7d). NPC-700 has better electrochemical properties than the biomass-based carbon materials that have been reported (Table. 1). The results show that the carbon content is high, the specific surface area is large, and the carbon material with rich pore diameter has broader application prospects.

**Table 1.** Comparison of specific capacitance of various carbon materials

Sample	Electrolyte	Current density (A/g)	Specific capacitance (F/g)	Ref.
ACGL	6 M KOH	0.5	364	[34]
DC-700	1 M KOH	0.5	320	[16]
NHPCS	1 M H <sub>2</sub> SO <sub>4</sub>	0.5	451	[17]
ACs	6M KOH	0.1	340	[18]
Tea leaves	2 M KOH	1.0	330	[35]
PF-700	6 M KOH	0.5	270	[36]
PNPC	6 M KOH	1.0	287.1	[6]
PC-1100	1 M LiPF <sub>6</sub>	1.0	250	[5]
PCSS	1 M KOH	0.1	243	[4]
NPC-700	6 M KOH	0.5	405	This work

#### 4. CONCLUSIONS

NPCs with high specific surface area were prepared by simple carbonization and activation using pine nut shells as raw materials. The specific surface area of the material can be well controlled by controlling the activation temperature. When the temperature is 700°C, the specific surface area of the material is as high as 2192 m<sup>2</sup>/g. The electrochemical performance of the NPC electrode material indicates that the NPC-700 has much better specific capacity and an excellent rate performance; its specific capacity retention rate is as high as 95% after 5000 cycles of testing. This work provides a

simpler and more effective method for the preparation of biomass-based nitrogen-doped porous carbon materials with great prospects in energy storage.

## ACKNOWLEDGMENTS

We thank LetPub ([www.letpub.com](http://www.letpub.com)) for its linguistic assistance during the preparation of this manuscript. The authors gratefully acknowledge support from the National Natural Science Foundation of China (5187011196, U1501242 and 51671062), National Key Research and Development Program (2018YFB1502103, 2018YFB1502105), Guangxi Bagui Scholar Foundation, Guangxi Collaborative Innovation Centre of Structure and Property for New Energy and Materials (2012GXNSFGA06002), Guangxi Science and Technology Project (AD17195073, 2017AD23029), and Guangxi Major Science and Technology Special Project (AA17202030-1). We also thank the Guangxi Advanced Functional Materials Foundation and Application Talents Small Highlands, and the Innovation Project of Guangxi Graduate Education (2019YCXS112), for providing financial support. F.R. is grateful to the Canada Research Chairs program for partial salary support.

## References

1. N. Zhang, N. Gao, C. Fu, D. Liu, S. Li, L. Jiang, H. Zhou, Y. Kuang, *Electrochim. Acta*, 235 (2017) 340-347.
2. Y. Chen, L. Sun, Z. Lu, Z. Liu, Y. Jiang, K. Zhuo, *Ionics*, 25 (2018) 2781-2789.
3. M. Yu, Y. Han, Y. Li, J. Li, L. Wang, *Carbohydr. Polym.*, 199 (2018) 555-562.
4. R. Xia, J. Zhou, X. Wu, J. Huang, *Mater. Lett.*, 216 (2018) 158-161.
5. J. Niu, R. Shao, J. Liang, M. Dou, Z. Li, Y. Huang, F. Wang, *Nano Energy*, 36 (2017) 322-330.
6. Y. Zhou, J. Ren, Y. Yang, Q. Zheng, J. Liao, F. Xie, W. Jie, D. Lin, *J. Solid State Chem.*, 268 (2018) 149-158.
7. K. Fang, J. Chen, X. Zhou, C. Mei, Q. Tian, J. Xu, C.-P. Wong, *Electrochim. Acta*, 261 (2018) 198-205.
8. J. Lao, P. Sun, F. Liu, X. Zhang, C. Zhao, W. Mai, T. Guo, G. Xiao, J. Albert, *Light: Science & Applications*, 7 (2018).
9. S. Liu, C. An, X. Chang, H. Guo, L. Zang, Y. Wang, H. Yuan, L. Jiao, *J. Mater. Sci.*, 53 (2017) 2658-2668.
10. X. Chang, L. Zang, S. Liu, M. Wang, H. Guo, C. Wang, Y. Wang, *J. Mat. Chem. A*, 6 (2018) 9109-9115.
11. D.-Y. Lee, G.-H. An, H.-J. Ahn, *J. Ind. Eng. Chem.*, 52 (2017) 121-127.
12. M. Vijayakumar, R. Santhosh, J. Adduru, T.N. Rao, M. Karthik, *Carbon*, 140 (2018) 465-476.
13. E. Frackowiaka, K. Jurewicza, S. Delpueuxb, F. BeÅguinb, *J. Power Sources*, 97-98 (2001) 822-825.
14. X. Liu, P. Song, B. Wang, Y. Wu, Y. Jiang, F. Xu, X. Zhang, *ACS Sustainable Chemistry & Engineering*, 6 (2018) 16315-16322.
15. F.O. Agyemang, G.M. Tomboc, S. Kwofie, H. Kim, *Electrochim. Acta*, 259 (2018) 1110-1119.
16. T. Wei, X. Wei, Y. Gao, H. Li, *Electrochim. Acta*, 169 (2015) 186-194.
17. C. Wang, D. Wu, H. Wang, Z. Gao, F. Xu, K. Jiang, *J. Colloid Interface Sci.*, 523 (2018) 133-143.
18. K. Wang, N. Zhao, S. Lei, R. Yan, X. Tian, J. Wang, Y. Song, D. Xu, Q. Guo, L. Liu, *Electrochim. Acta*, 166 (2015) 1-11.
19. R.E.H. Sims, H.-H. Rogner, K. Gregory, *Energy Policy*, 31 (2003) 1315-1326.
20. C. Wang, Y. Xiong, H. Wang, Q. Sun, *J. Colloid Interface Sci.*, 528 (2018) 349-359.
21. T. Wu, L. Suna, F. Xua, D. Cai, *J. Mater. Sci. Technol.*, (2018) 2384–2391.
22. D. Luo, P. Han, L. Shi, J. Huang, J. Yu, Y. Lin, J. Du, B. Yang, C. Li, C. Zhu, J. Xu, *Appl. Surf. Sci.*,

- 462 (2018) 713-719.
23. C. Peng, T. Zeng, Y. Yu, Z. Li, Z. Kuai, W. Zhao, *J. Mater. Sci.: Mater. in Electronics*, 29 (2018) 18674-18683.
24. J. Ruan, T. Yuan, Y. Pang, S. Luo, C. Peng, J. Yang, S. Zheng, *Carbon*, 126 (2018) 9-16.
25. W. Si, J. Zhou, S. Zhang, S. Li, W. Xing, S. Zhuo, *Electrochimica Acta*, 107 (2013) 397-405.
26. C. Guo, N. Li, L. Ji, Y. Li, X. Yang, Y. Lu, Y. Tu, *J. Power Sources*, 247 (2014) 660-666.
27. L. Zhang, Z. Su, F. Jiang, L. Yang, J. Qian, Y. Zhou, W. Li, M. Hong, *Nanoscale*, 6 (2014) 6590-6602.
28. K. Xiao, L.-X. Ding, H. Chen, S. Wang, X. Lu, H. Wang, *J. Mat. Chem. A*, 4 (2016) 372-378.
29. C. Shao, Z. Wang, E. Wang, S. Qiu, H. Chu, Y. Zou, C. Xiang, F. Xu, L. Sun, *New J. Chem.*, 41 (2017) 12901-12909.
30. Z. Li, Z. Xu, X. Tan, H. Wang, C.M.B. Holt, T. Stephenson, B.C. Olsen, D. Mitlin, *Energy Environ. Sci.*, 6 (2013) 871.
31. Z. Wen, X. Wang, S. Mao, Z. Bo, H. Kim, S. Cui, G. Lu, X. Feng, J. Chen, *Adv. Mater.*, 24 (2012) 5610-5616.
32. D. He, W. Zhao, P. Li, Z. Liu, H. Wu, L. Liu, K. Han, L. Liu, Q. Wan, F.K. Butt, X. Qu, *Appl. Surf. Sci.*, 465 (2019) 303-312.
33. X. Xu, Y. Liu, M. Wang, C. Zhu, T. Lu, R. Zhao, L. Pan, *Electrochim. Acta*, 193 (2016) 88-95.
34. E. Hao, W. Liu, S. Liu, Y. Zhang, H. Wang, S. Chen, F. Cheng, S. Zhao, H. Yang, *J. Mat. Chem. A*, 5 (2017) 2204-2214.
35. C. Peng, X.-b. Yan, R.-t. Wang, J.-w. Lang, Y.-j. Ou, Q.-j. Xue, *Electrochim. Acta*, 87 (2013) 401-408.
36. B. Liu, Y. Liu, H. Chen, M. Yang, H. Li, *J. Power Sources*, 341 (2017) 309-317.